Control of Rotor Tip Leakage Through Cooling Injection From the Casing in a High-Work Turbine

Thomas Behr
Turbomachinery Laboratory,
ETH Zurich,
CH-8092 Zurich, Switzerland
e-mail: behr@lsm.iet.mavt.ethz.ch

Anestis I. Kalfas
Department of Mechanical Engineering,
Aristotle University of Thessaloniki,
GR-54124 Thessaloniki, Greece

Reza S. Abhari
Turbomachinery Laboratory,
ETH Zurich,
CH-8092 Zurich, Switzerland

This paper presents an experimental investigation of a novel approach for controlling the rotor tip leakage and secondary flow by injecting cooling air from the stationary casing onto the rotor tip. It contains a detailed analysis of the unsteady flow interaction between the injected air and the flow in the rotor tip region and its impact on the rotor secondary flow structures. The experimental investigation has been conducted on a one-and-1/2-stage, unshrouded turbine, which has been especially designed and built for the current investigation. The turbine test case models a highly loaded, high pressure gas turbine stage. Measurements conducted with a two-sensor fast-response aerodynamic probe have provided data describing the time-resolved behavior of flow angles and pressures, as well as turbulence intensity in the exit plane of the rotor. Cooling air has been injected in the circumferential direction at a 30 deg angle from the casing tangent, opposing the rotor turning direction through a circumferential array of ten equidistant holes per rotor pitch. Different cooling air injection configurations have been tested. Injection parameters such as mass flow, axial position, and size of the holes have been varied to see the effect on the rotor tip secondary flows. The results of the current investigation show that with the injection, the size and the turbulence intensity of the rotor tip leakage vortex and the rotor tip passage vortex reduce. Both vortices move toward the tip suction side corner of the rotor passage. With an appropriate combination of injection mass flow rate and axial injection position, the isentropic efficiency of the stage was improved by 0.55 percentage points. [DOI: 10.1115/1.2777185]

Introduction

Modern gas turbine designs aim to reach the highest possible turbine entry temperatures in order to increase cycle efficiency and turbine specific work. Different cooling strategies have been developed in order to achieve adequate life for all components that are exposed to these high temperature gas flows. One critical region for cooling in a high-pressure turbine is the blade tip area, which experiences high thermal loads and which is difficult to cool. A second aspect in optimizing turbine efficiency is the reduction of aerodynamic losses. The unshrouded design of high-pressure rotor blade rows introduces high losses due to tip leakage flows. Booth [1] found tip leakage losses to be in the order of up to one-third of the overall stage losses.

Several strategies for reducing losses due to blade tip gap flows have been the subject of a number of investigations over the past decade. According to Denton [2], the loss related to tip leakage flows is proportional to a discharge coefficient. Further, the loss scales with the velocity distribution around the blade tip, and thus with the loading of the blade tip.

One way of changing the discharge coefficient without affecting significantly the pressure distribution around the tip profile is to modify the blade tip geometry. Contouring can be done by including squealer rims or radii along the edges of the tip. Booth [3] presented test on a series of different tip geometries and evaluated the related discharge coefficients. Bindon and Morphis [4] tested three different tip geometries in a linear cascade. They found that the discharge coefficient is not necessarily representa-

tive of the overall loss associated with the tip leakage flow. It does not account for losses due to mixing of the tip leakage flow downstream of the rotor. In the investigation of Kaiser and Bindon [5] in a 1.5-stage rotating rig, the plain tip was shown to have the best performance compared to other geometries tested. With a tip that is radiused along the edges of the pressure side, the vena contracta that usually forms inside the tip gap could be almost completely eliminated. Other studies in rotating rigs concerning this area of research have been presented by Yoshino [6] and Camci et al. [7]. A numerical analysis examining the influence of improved tip concepts has been described by Mischo et al. [8] and Chander et al. [9].

The possibility of reducing tip leakage flows through a reduced loading of the tip region has been discussed by De Cecco et al. [10] and Yamamoto et al. [11]. Staubach et al. [12] achieved the off-loading of the tip by applying 3D design strategies to the profiles. Tip lean was found to be beneficial for this purpose; however, its application is limited due to stresses within the rotor blade.

Offenburg et al. [13] investigated the effect of different trenches within the casing around the rotor on efficiency of the stage. The function of trenches within the casing was found to be dependent on the tip gap height. Up to a relative tip gap of 2.3% blade span, a straight casing contour has been shown to yield the best results.

On the effect of tip leakage in a multistage environment, Harvey [14] concluded that no benefit results from the tip leakage flow once it has formed into a vortex. In order to limit the losses that this vortex generates in subsequent blade rows, the tip leakage flow and thus the strength of the vortex have to be reduced.

Another approach in order to reduce the losses due to tip leakage has been examined by Dey and Camci [15] and Rao and Camci [16,17]. Coolant was injected from the blade tip into the tip gap in order to reduce the mixing losses due to the tip leakage.

Jets at different discrete positions and blowing ratios were evaluated. An influence of the injection rate on the radial position of the tip leakage vortex and of the injection position on its strength could be detected.

The concept of injecting air from the rotor casing through circumferential slots onto the rotor blade tip was proposed by Auyer [18]. Minoda et al. [19] injected air in a similar way through arrays of inclined holes at three axial positions. The inclined jets at an angle of 30 deg opposed the rotor turning direction. It was found that the flow could be influenced down to a radial position of 50% span; across this range, the relative rotor exit angles were increased from 100% to 70% span and reduced from 70% to 50% span. The promising observations of these investigations are based on steady state measurements in the stator relative frame.

In gas turbine engines, the external side of the high-pressure turbine rotor casing is generally cooled with compressor discharge air. The cooling is necessary for the casing part to withstand the temperatures of the rotor inlet gas that may be 1400°C and higher. After cooling the casing, the cooling air is purged into the gas path of the turbine, where it mixes out with the main flow. The current approach investigates the injection of cooling air from the rotor casing onto the rotor tip. This injection is used to control and reduce the development of the rotor tip secondary flows and hence improve the aerodynamic performance. In contrast to previous work and to understand the aerodynamics of this complex problem, unsteady measurement techniques are applied, which allow a study of the time-resolved flow in the rotor-relative frame. This experimental approach is supported by a numerical study by Mischo et al. [20].

Experimental Method

Turbine Test Rig Facility. The experiments for the current investigation have been conducted on the 1.5-stage unshrouded axial turbine test rig at the Turbomachinery Laboratory of ETH Zurich. A cross section view of the turbine module is presented in Fig. 1. Global parameters of the turbine at the design operating point are shown in Table 1. The characteristics of each blade row are presented in Table 2.

The air loop of the facility is of a quasiclosed type and includes a radial compressor, a two-stage water to air heat exchanger, and a calibrated venturi nozzle for mass flow measurements. Before the flow enters the turbine section, it passes through a 3 m long straight duct, which contains flow straighteners to ensure an evenly distributed inlet flow field. Downstream of the turbine, the air loop is open to atmosphere. A dc generator converts the turbine power and controls the rotational speed of the turbine. A torque meter measures the torque that is transmitted by the rotor shaft to the generator. The turbine entry temperature is controlled to an accuracy of 0.3% and the rpm is kept constant within ± 0.5 min^{-1} by the dc generator. The pressure drop across the turbine is stable within 0.3% for a typical measurement day. More detailed information on the test rig can be found in Ref. [21].

Measurement Techniques. The flow field data presented in the paper are derived from time-resolved probe measurements in a plane 15% rotor axial chord downstream of the rotor trailing edge. The unsteady pressure measurement technology of the fast-response aerodynamic probes (FRAPs) has been developed at the LSM (Kupferschmied et al. [22] and Pfau et al. [23]). The mainstream flow field was measured using a novel 1.8 mm tip diameter, two-sensor FRAP in virtual-four-sensor mode to provide two-dimensional, time-resolved flow field information. Each measurement plane is resolved by a grid of 27 points in the radial direction clustered close to the end walls, and 20 equally spaced points in the circumferential direction, covering one stator pitch. The time-resolved pressure signals are acquired at each measurement point at a sampling rate of 200 kHz over a period of 2 s. The data sets are processed to derive basic flow quantities, i.e., total and static pressures, flow yaw and pitch angles, velocity compo-
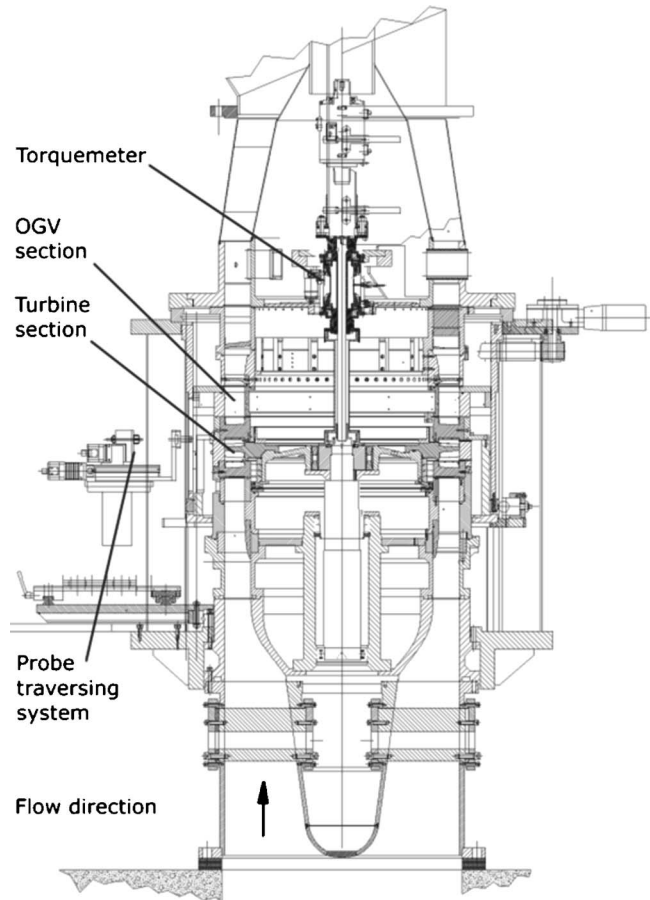

Fig. 1 "LISA" 1- and −1/2-stage axial turbine facility

nents, and Mach number, by applying a phase lock average over 85 rotor revolutions. For the data evaluation, three consecutive rotor passages were selected. Each rotor pitch is resolved in time by 82 samples. The frequency response of the probe allows flow features to be captured at frequencies up to 35 kHz. With this two-sensor probe technology, it is also possible to determine flow turbulence information (Porreca et al. [24]). The FRAP technology also provides temperature data at a frequency of up to 10 Hz.

The time-resolved static pressure distribution of the base line configuration at the rotor casing has been measured using miniature piezoresistive differential pressure transducers (Endevco 8507C-5) having a head diameter of 2.67 mm and a resonance frequency of 85 kHz. A sector of the rotor casing of the size of

Table 1 Main parameter of "LISA" 1.5-stage axial turbine research facility at design operating point (measured)

Turbine	
Rotor speed (rpm)	2700
Pressure ratio (1.5 stage, total to static)	1.60
Turbine entry temperature (°C)	55
Total inlet pressure (bar abs norm)	1.4
Mass flow (kg/s)	12.13
Shaft power (kW)	292
Hub/tip diameter (mm)	660/800
First stage	
Pressure ratio (first stage, total to total)	1.35
Degree of reaction (—)	0.39
Loading coefficient $\psi = \Delta h / u^2$ (—)	2.26
Flow coefficient $\phi = c_x / u$ (—)	0.65

Table 2 Characteristic geometry and performance parameters of the 1.5-stage turbine configuration (performance values are derived from five-hole-probe measurements at the design operating point)

	Stator 1	Rotor	Stator 2
Number of blades	36	54	36
Inlet flow angle (deg) (midspan)	0	54	−42
Exit flow angle (deg) (midspan)	73	−67	64
Aspect ratio (span/chord)	0.87	1.17	0.82
Blade row relative exit Mach numbers (—) (average)	0.54	0.50	0.48
Reynolds number based on true chord and blade row relative exit velocity (—)	7.1×10^5	3.8×10^5	5.1×10^5

Table 3 Geometric parameters of injection configurations

Configuration	A	B	C
Rotor axial chord	30	50	30, 50
Number of holes/rotor	10	10	10+10
Hole diameter (mm)	1.0	1.0	0.7
Hole angle relative to	30	30	30
Length/diameter ratio	8.0	8.0	11.4

one stator pitch has been resolved with a mesh of 7 axial and 40 equidistant circumferential positions. Data from all sensors have been acquired simultaneously at a sampling rate of 100 kHz.

Cooling Air Injection. The cooling air injection is applied through an injection window that covers a sufficiently representative sector of five rotor pitches. A picture of the injection window arrangement is shown in Fig. 2. The inner contour of the rotor casing ring and the injection window have been machined together in order to ensure a continuous inner contour. The part of the window that faces the rotor tip area is interchangeable. In this way, different injection plate configurations can be tested with a short changeover time.

The cooling air is provided by both an air supply system that dehumidifies the air and controls the temperature and the mass flow. A detailed description of the system can be found in Ref. [25]. In order to achieve a uniform distribution of the injected air, the injection window module has a symmetric shape. The air enters the plenum of the module from two sides. To further homogenize the air, the plenum is divided into two chambers. The air enters Plenum 1, before it passes through a screen of 3×40 large holes to reach Plenum 2. The total pressure and total temperature are measured in Plenum 2.

For the current investigation, three axial injection positions were tested (Table 3). The axial positions were chosen to counteract the formation of the tip leakage vortex. With all configurations, air is injected circumferentially against the rotor turning direction at an angle of 30 deg relative to the casing's tangent in order to oppose the rotor tip leakage flow. For each configuration,
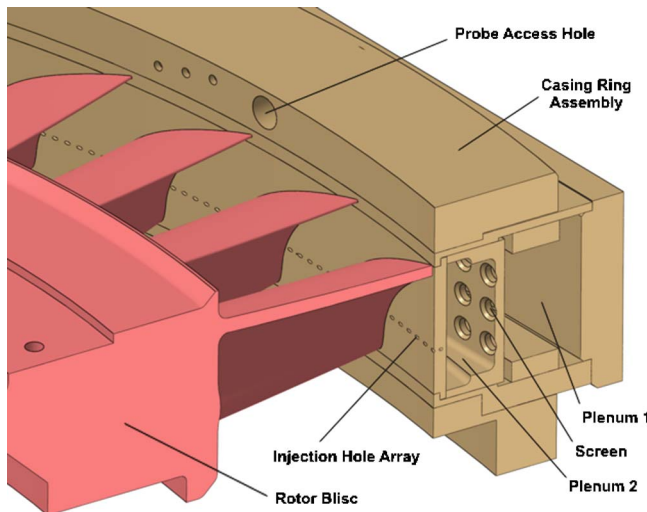
cooling air is injected at two mass flow rates representing an injection of 0.7% and 1.0% of the turbine mass flow on the full annulus at the conditions shown in Table 4. Differences between the discharge characteristics of the injection configurations have been found to be negligible. Reference measurements for all three configurations with no injection are made with the holes sealed from the inside of the plenum with tape.

Rotor Tip Flow and Casing Injection

In axial flow turbines, the required clearance between the tips of the rotor blades and the surrounding casing results in secondary flows. Fluid that passes through the tip gap of the rotor forms a tip leakage vortex, which has a major contribution to the loss production inside the rotor. A detailed literature review on the studies of tip clearance flow in unshrouded axial turbines has been presented by Sjolander [26]. The following section gives an overview of the secondary flow phenomena in the rotor blade row of the turbine configuration under investigation. In the following, the problem of the casing air injection will be addressed. Based on the experimental findings, the interaction between rotor secondary flows and injection fluid will be discussed.

In Fig. 3, a schematic view of the secondary flow development inside a rotor is shown. The incoming boundary layers at the hub and tip end wall experience a strong adverse pressure gradient as

Table 4 Injection air conditions

Injection rate (% of passage mass flow)	0.7	1.0
Plenum total pressure $p_{t,I}$ (kPa)	128	140
Plenum total temperature $T_{t,I}$ (°C)	32.5	32.5
Average density ratio DR (—)	1.0	1.0
Average blowing ratio BR (—)	2.2	3.2
Average momentum flux ratio IR (—)	4.8	10.3

Fig. 2 Air injection system and probe access within traversable rotor casing ring assembly
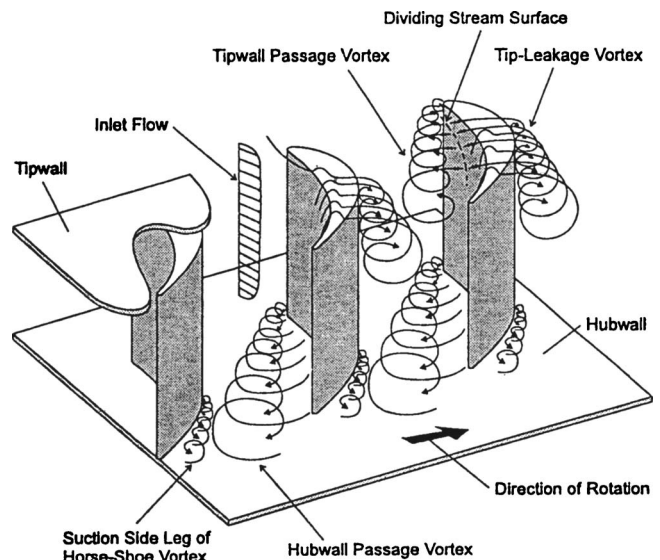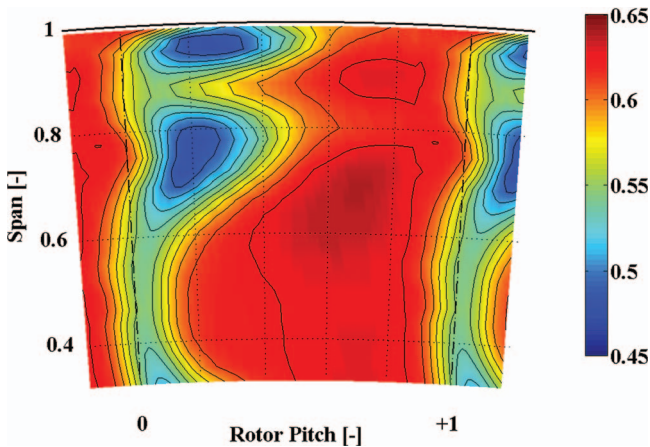

Fig. 3 Secondary flow model after Sjolander [26]

Fig. 4 Relative total pressure coefficient $C_p t_{rel}$ (-) measured at the rotor exit (rotor-relative frame, time averaged)

Fig. 5 rms of nondeterministic pressure variation (Pa) measured at the rotor casing (rotor-relative frame, time averaged)

they approach the leading edge of the rotor, which leads to the formation of a "horseshoe" vortex that wraps around the profile. The incoming end wall flow that enters the passage is influenced by the pressure gradient between the pressure and suction sides. Due to the difference in momentum across the boundary layer, the pressure gradient drives the fluid that is adjacent to the end wall closer to the suction side. This crossflow on the end wall subsequently rolls up into the passage vortex, which often merges with the pressure side leg of the horseshoe vortex.

In the tip region of an unshrouded rotor blade, the characteristics of secondary flows differ from the previously described model. Due to the reduced strength of the adverse pressure gradient at the tip gap, the horseshoe vortices appear only at small clearances. In addition, a tip leakage vortex develops. At the blade tip, the pressure gradient between pressure and suction side sucks off mass flow from the tip region of the pressure side into the tip gap. The inlet flow to the gap separates along the pressure side corner of the tip gap and forms a separation bubble. The unseparated flow passes through a vena contracta that is between the separation bubble and the casing. This vena contracta region is characterized by a maximum in the flow velocity and a minimum in the static pressure.

The tip leakage flow leaves the gap at a high velocity and interacts with the flow on the blade suction side. The passage flow and the passage vortex cause the leakage jet to roll up into the tip leakage vortex. In the rotor exit plane, this counter-rotating pair of tip leakage vortex and tip passage vortex are observed to be attached to the suction side. The tip leakage vortex is additionally confined by the casing end wall.

In Fig. 4, the position of the secondary flows in the rotor tip region can be confirmed from the distribution of the relative total pressure coefficient. In this plane at 15% rotor axial chord downstream of the rotor trailing edge, the vortices can be identified as regions of low relative total pressure. Hence, the tip leakage vortex extends from 90% to 100% span, adjacent to the tip passage vortex from 60% to 90% span. Further, radially inward on the left side of the vortices, the low-pressure field of the rotor wake can be identified. A more detailed discussion of the flow field has been presented in Ref. [21].

Figure 5 shows the nondeterministic pressure distribution at the casing wall measured with fast-response pressure sensors. The value plotted represents the variation (or rms) of the phase-locked pressure signal $\sigma(p'_w)$ calculated out of 180 values. The distribution of this parameter has been calculated for each stator-rotor relative position. Afterward, all these distributions have been averaged in the rotor-relative frame. At the position of the vena contracta and the separation bubble at the pressure side corner of the tip, a region with high levels of pressure unsteadiness can be
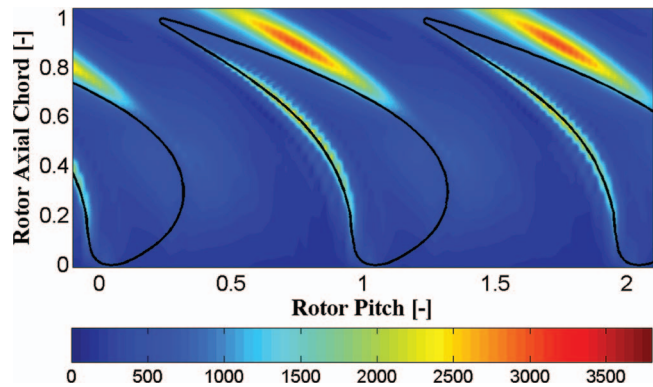
found from 20% to 80% axial chord. This region marks the position where the tip leakage fluid enters the tip gap. At the opposite side of the tip, the region of the tip leakage vortex can clearly be distinguished. The position of the start of the vortex development at 60% rotor axial chord coincides with the approximate position of the peak suction pressure. Inside the vortex region, the maximum level of unsteadiness is at a position of 90% rotor axial chord. Xiao and Lakshminarayana [27] investigated the development of tip leakage vortices using laser Doppler velocimetry (LDV). They found that a reduction of the vortex circulation downstream 90% rotor axial chord coincided with a slower growth of the vortex. If one assumes that the circulation and the unsteadiness of a vortex are correlated, this effect is also seen in the present measurement.

Due to the fact that the rotor is embedded in between two stators, the rotor exit flow as well as the development of rotor secondary flows are influenced by blade row interactions. Figure 6 shows the nondeterministic pressure distribution on the rotor casing at 104% rotor axial chord versus the time of two stator blade passing periods. The tip leakage vortex is again indicated by high levels of pressure unsteadiness. The relative circumferential position of the tip leakage vortex to the rotor trailing edge varies with its position relative to the subsequent stator leading edge. The unsteady casing pressure measured further upstream shows that the blade row interaction affects the development of the entire tip leakage vortex up to the position where the vortex first leaves the tip gap. This effect is seen in a modulation of unsteadiness and a variation of the relative position of the vortex. This phenomenon is also discussed in Ref. [21].
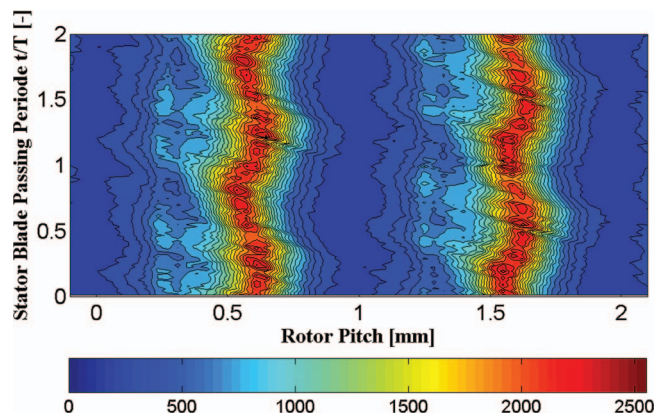

Fig. 6 rms of nondeterministic pressure variation (Pa) measured at the rotor casing at 104% rotor axial chord versus stator blade passing period (rotor-relative frame)
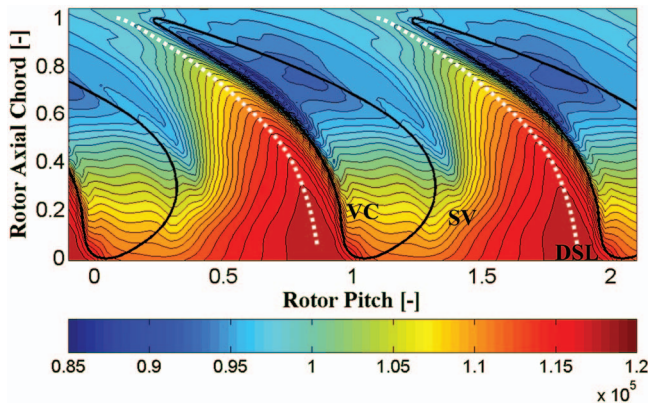
Fig. 7 Static pressure (Pa) measured at the rotor casing (rotor-relative frame, time averaged)

Fig. 9 Model of the flow directions at the casing in the rotor-relative frame of reference

The acceleration of the flow into the tip gap reduces the static pressure close to the pressure side. The maximum static pressure at the tip occurs along the dividing stream surface (see Fig. 3) that is close to the blade pressure side. Fluid on one side of this surface goes into the tip gap. The fluid on the other side forms the cross-passage flow that is then accelerated toward the suction side and forms the passage vortex. Another secondary flow feature develops at the tip of rotating blade rows (not shown in Fig. 3) and is caused by the relative movement of the blade to the tip casing wall. The casing boundary layer is scraped by the suction side of the blade tip and moves down the suction surface. This shear layer eventually rolls up into the scraping vortex, which rotates counter to the tip leakage vortex. The scraping vortex results in a low static pressure region at the end wall.

The previously described secondary flow features at the casing are evident in the distribution of static pressure at the casing (see Fig. 7). The trace of the dividing stream surface at the casing is indicated by the static pressure maxima of the dividing stream line (DSL) that is offset from the pressure side toward the passage. On the pressure side, a line of static pressure minima is also seen and is a result of the vena contracta (VC) region. A second line of static pressure minima, which is offset from the suction side toward the passage, is caused by fluid that has been accelerated due to the proximity of the blade. This fluid goes along the suction surface, and is referred to as the scraping vortex (SV).

The oil flow visualization near the pressure side on the blade tip surface (Fig. 8) shows the position of the line of the separation bubble as well as the flow direction across the separation bubble. The region along the pressure side corner of the tip is blank, whereas further inward oil deposits from the recirculation are seen.

In summary, the interaction between the injected fluid and the main flow can be subdivided into two regions. These regions are
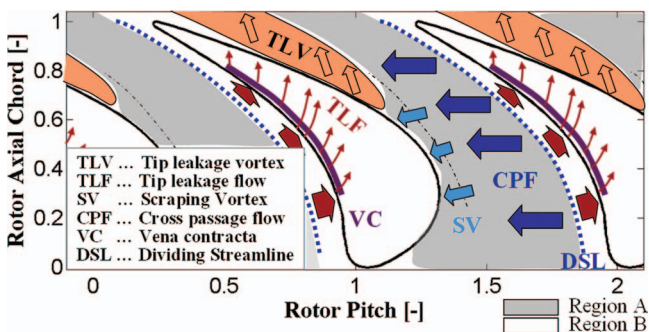
distinguishable depending on the manner in which the injected fluid enters the main flow path. Region A (shown as the gray shaded region in Fig. 9) is comprised of the cross flow from the pressure side to the suction side and the SV that is close to the suction side. Fluid in this region tends to move from the pressure to the suction side across the passage in the rotor-relative frame of reference. Region B is dominated by the fluid that passes through the tip clearance and eventually forms the tip leakage vortex. This region extends circumferentially from the dividing stream surface close to the suction side across the rotor tip until the rotor tip suction side. It further includes the region downstream of the rotor suction side, which is dominated by the tip leakage vortex. The flow in this region moves faster in the circumferential direction than the rotor. Therefore, it moves in the opposite circumferential direction in the rotor-relative frame then the flow of region A.

The mass flow rate of the cooling air injection is determined by the pressure difference between the plenum total pressure and the static pressure at the exit of the injection hole and the discharge coefficient. Each injection hole is exposed to a static pressure field that varies with the relative position of the rotor blades. Thus, the injection mass flow rate changes accordingly. The maximum mass flow occurs with the lowest static pressure and vice versa. Figure 10 shows the circumferential distribution of static casing pressure at the two axial injection positions considered in the current investigation. The vertical blue lines in the plots mark the approxi-
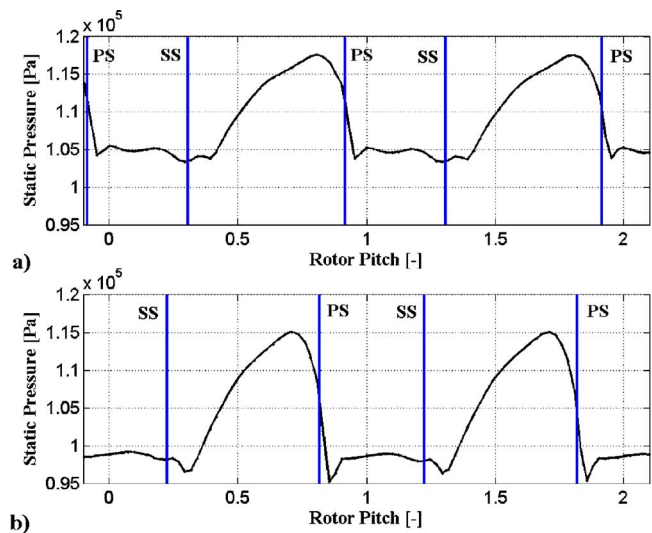

Fig. 8 Flow visualization on rotor tip surface

Fig. 10 Static pressure distribution measured at the rotor casing (rotor-relative frame, time averaged) at two rotor axial chord positions; (*a*) 30% and (*b*) 50%
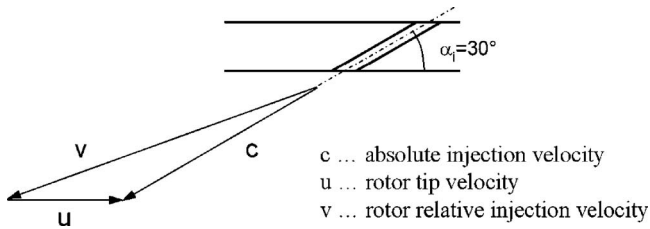
Fig. 11 Velocity triangle of casing injection

c ... absolute injection velocity
u ... rotor tip velocity
v ... rotor relative injection velocity
$\alpha_i = 30°$

mate positions of the pressure and suction sides. It is evident that on the surface of the blade tip, the highest injection rate occurs at relatively constant level. Within the passage, the injection rate reduces from this level until the dividing stream surface that is close to the pressure side at which the static pressure reaches its maximum.

The inclined injection at an angle of 30 deg introduces a circumferential velocity component that is opposite to the rotor turning direction. In the rotor-relative frame, the injection angle is reduced to approximately 20 deg relative to the casing tangent. The velocity triangle of the injection is shown in Fig. 11.

In order to show the evolution of the injected fluid within the rotor passage, the axial velocity in the rotor exit plane can be considered. Figure 12(a) shows the distribution of axial velocity of the base line case. The midpassage flow of the rotor has an average axial velocity of around 70 m/s. The regions occupied by the tip leakage vortex and tip passage vortex show a reduction of axial velocity of up to 30%. Figure 12(b) visualizes the change in
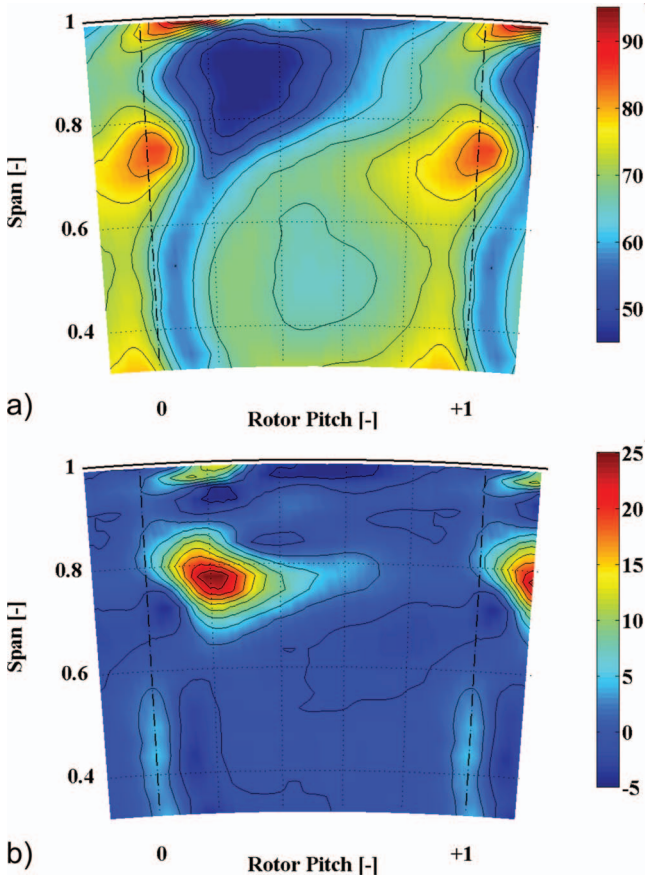

Fig. 12 Rotor-relative frame, time-averaged contours: (a) axial velocity c_x (m/s) measured at the rotor exit, baseline, (b) axial velocity difference Δc_x (m/s) measured at the rotor exit between injection A-1% and base line case

axial velocity due to an injection of 1% cooling mass flow at 30% rotor axial chord (injection configuration A). The velocity change is the difference between the axial velocities of the injection and the base line case. The mass flow difference derived from the measured data of both flow fields is equivalent to the injected mass flow. A substantial increase in axial velocity is seen in the core of the tip passage vortex (see also Fig. 4). Also, in the region of the tip leakage vortex, there is a slight increase. The rest of the flow field is nearly unaffected. This indicates that at the exit of the rotor, most of the injected fluid has accumulated within the tip passage vortex.

Based on the flow models and experimental data described above, the main effects of cooling air injection can be described as follows:

(1) Within the tip gap region until the dividing stream surface, the cooling jets oppose the direction of the tip leakage fluid. Due to the momentum exchange between the jets and the leakage fluid and the increased static pressure upstream of the holes, the leakage fluid is reduced and deflected to a more downstream position. Therefore, the leakage vortex leaves the suction side at a more downstream position. Within the rotor exit plane, the vortex has a reduced strength and is closer to the suction side.

(2) The upstream border of the passage vortex marks the position of an end wall separation line, where the boundary layer of the incoming flow and the new boundary layer of the cross-passage flow meet each other. This separation line moves upstream due to the casing air injection, such that the secondary flow of the passage vortex then impinges on the suction side of the opposing blade at a more upstream position. The reason for this effect is the increase in static pressure upstream of the injection holes, which displaces the incoming low momentum fluid. Secondly, the injection is directed in the same direction as the cross-passage flow. Therefore, it will add to it a circumferential velocity component, which will accelerate the development of the passage vortex.

In the next section, this description of the flow is verified with experimental data.

Effect of the Injection Mass Flow

For all injection configurations considered in this investigation, the following effects are seen and are more pronounced with *increasing* injection.

Tip Leakage Vortex and Tip Passage Vortex

Reduction of Vortex Turbulence Intensity. The position and the size of secondary flow features in the flow field can be identified from the turbulence intensities derived from the FRAP data. The distributions of turbulence intensity have been calculated for each measured stator-rotor relative position and then averaged in the rotor-relative frame. The measurements at the rotor exit of the base line case are presented in Fig. 13(a). The turbulence levels correlate well with the relative total pressure shown in Fig. 4. At the position of the tip leakage vortex, the highest turbulence levels are measured, and high levels are also seen in the region of the tip passage vortex.

With injection, the levels of turbulence intensity in the region of the rotor tip vortices are reduced by up to 35%. This effect is shown from the turbulence intensity differences of two cases with different injection mass flows in Figs. 13(b) and 13(c). The largest reduction of turbulence is in the tip passage vortex, as can be seen in blue contours at around 70% span. Hence, the injected fluid stabilizes the passage vortex.

In the region of the tip leakage vortex, a similar effect is seen; however, the largest reduction in turbulence occurs at midpitch and not at the center of the leakage vortex in the base line case
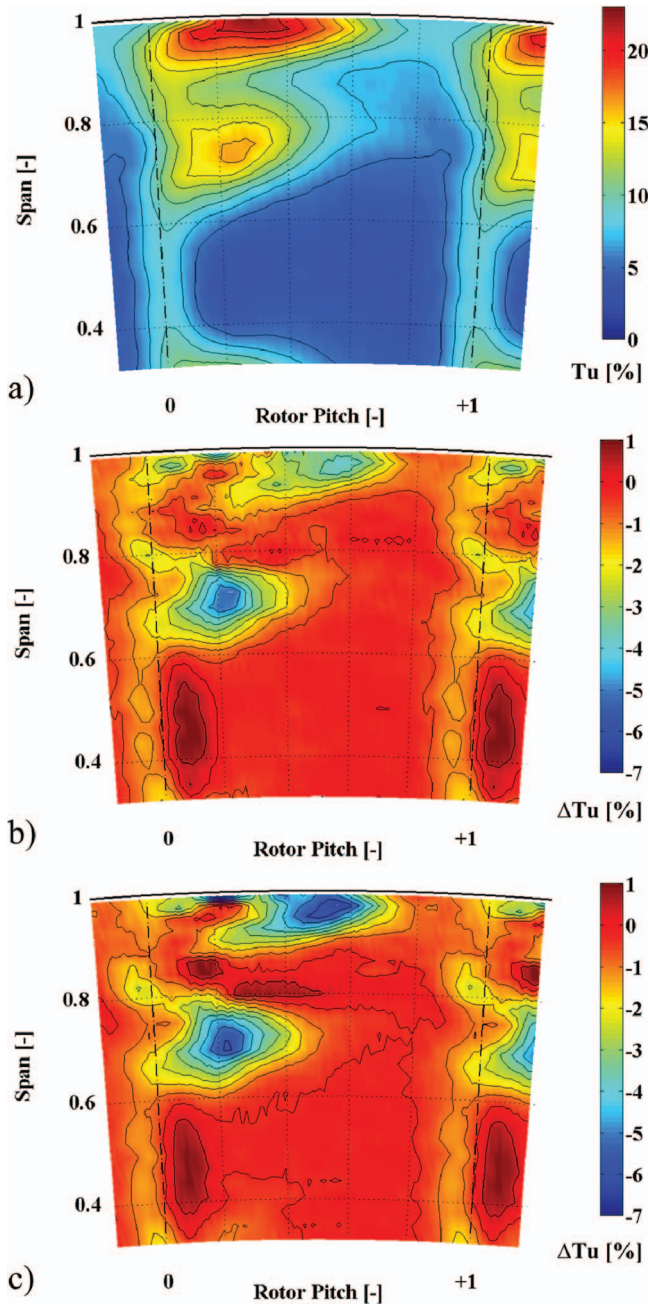
Fig. 13 Rotor-relative frame, time-averaged contours, injection configuration A; (*a*) turbulence Tu [%] measured at the rotor exit, baseline case, (*b*) turbulence difference ΔTu (%) measured at the rotor exit between injection A-0.7% and base line case, and (*c*) turbulence difference ΔTu (%) measured at the rotor exit between injection A-1% and base line case
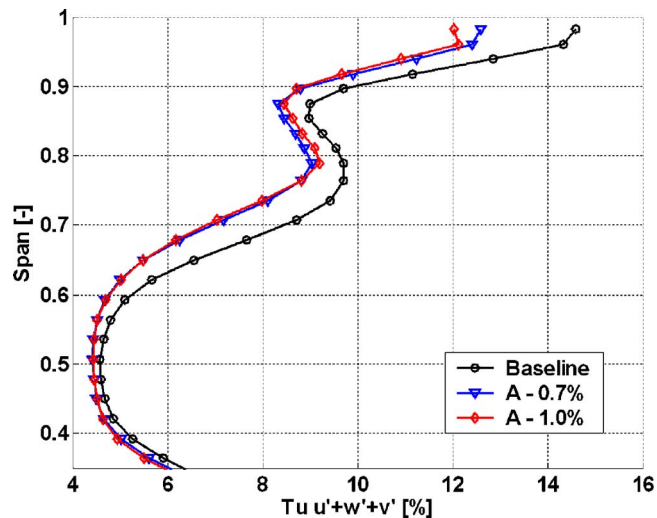

Fig. 14 Turbulence intensity (%) measured at the rotor exit (pitchwise mass averaged) of baseline case and injection configuration A at injection rates of 0.7% and 1.0%

gions, with reductions at around 2% for the tip leakage vortex and 1.5% for the tip passage vortex at an injection rate of 1% of the turbine mass flow.

Reduction of Vortex Size. The effect of the casing air injection on the vortex size has been described above. Another indication of this is seen in the pitchwise mass-averaged distribution of the flow yaw angle (see Fig. 15). In the flow region from 60% to 100% span, the characteristic overturning-underturning of the flow due to rotation of the vortices can be seen. The position of the minimum underturning due to the tip passage vortex is at around 75% span. This position moves radially outward with an increasing injection rate. Cooling injection of 1% of the turbine mass flow displaces the minimum by 4% span compared to the base line. This observation indicates that the passage vortex affects less fluid in the midspan region.

Increase of Vortex Overturning-Underturning. A second effect is seen in the distribution of flow yaw angles in Fig. 15. With an increasing injection rate, the underturning of the tip passage vortex and the overturning of tip leakage and tip passage vortex are

(see Figs. 13(*b*) and 13(*c*)). It is thought that the injection reduces the vortex diameter. Hence, the vortex moves closer to the suction side of the blade and occupies less space in the midpitch region. Since the turbulence levels are reduced in the entire region from 90% to 100% span, it is concluded that the tip leakage vortex is changed not only in size and position but also reduces its turbulence intensity.

To quantify the overall effect on the flow field, the pitchwise mass-averaged values are presented in Fig. 14. The largest reductions of turbulence intensity are also seen in the vortex span re-
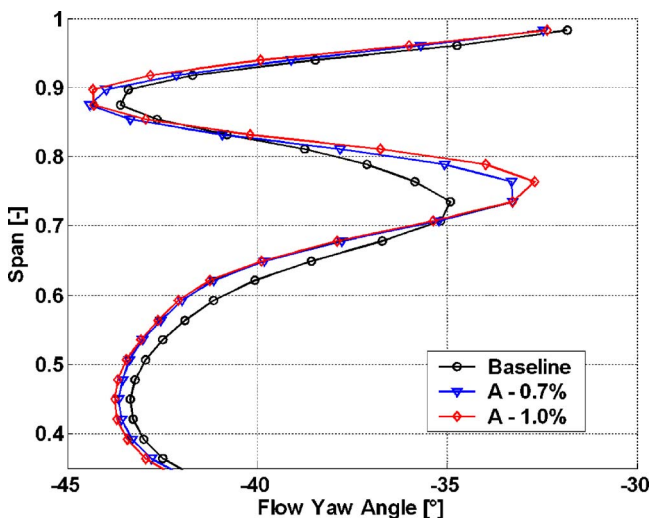

Fig. 15 Absolute yaw angle (%) measured at the rotor exit (pitchwise mass averaged) of baseline case and injection configuration A at injection rates of 0.7% and 1.0%
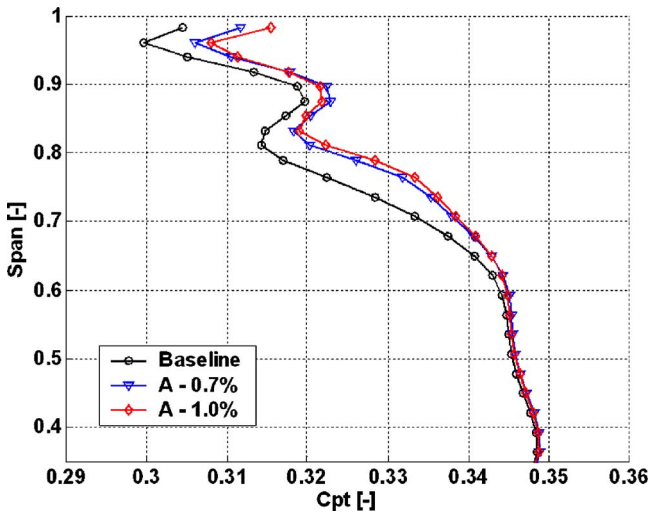
Fig. 16 Total pressure coefficient $C_p t$ (-) measured at the rotor exit (pitchwise mass averaged) of baseline case and injection configuration A at injection rates of 0.7% and 1.0%

Fig. 18 Flow yaw angle at 50% span (deg) measured at the rotor exit for base line case and two injection mass flows (rotor-relative frame)

increased. This indicates that the casing injection increases the rotation of the tip passage vortex, which results in larger deviation of the flow from the design.

Increase of Total Pressure. The injection of cooling air from the casing adds energy to the flow, which increases the total pressure in the affected region. Figure 16 shows the pitchwise mass-averaged distribution of total pressure. An effect of the injection on the main flow is seen in the region between the casing and 60% span. The largest increase in total pressure occurs at the positions of the vortex centers, that is, at 75% and close to the casing end wall.

Rotor Wake

Shift Away From Suction Side. The injection of casing cooling air is seen to have secondary effects on other secondary flow features such as the rotor wake. In Fig. 17, the pitchwise distribution of axial velocity at the midspan of the rotor exit is presented. The wake of the rotor is identified from the deficit of the axial velocity that is a minimum at a rotor pitch position of 0.08. The wake is clearly displaced away from the suction side as the injection rate is increased (see also Fig. 12(b)). This suggests that the
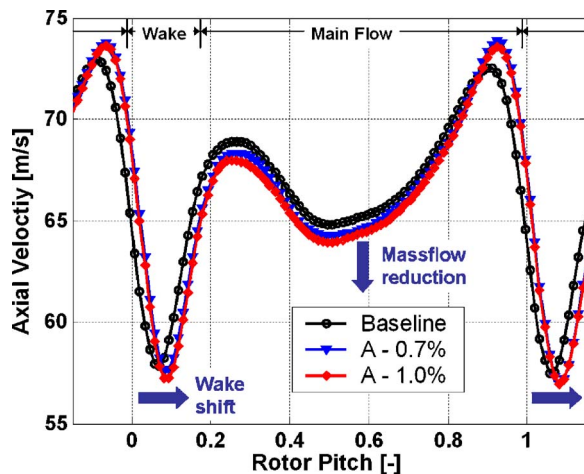

Fig. 17 Axial velocity c_x at 50% span (m/s) measured at the rotor exit for base line case and two injection mass flows (rotor-relative frame)
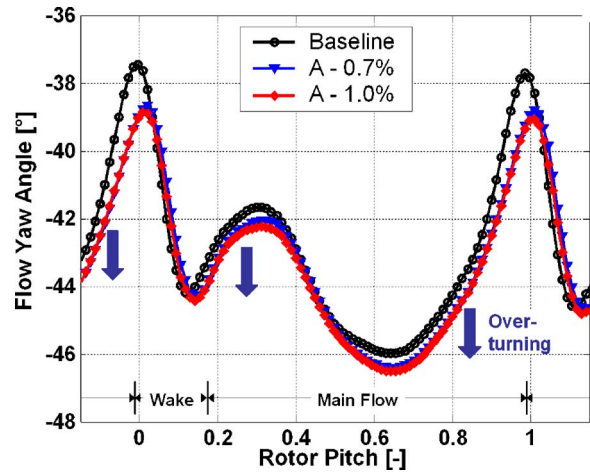
development of the suction side boundary layer on the rotor blade is altered in the presence of injection. It is thought that the modified passage vortex has an effect on the pressure distribution on the blade surface. The changed 3D loading on the blade then modifies the boundary layer and the wake development.

Increased Turning. In addition to the displacement of the wake, a change in the yaw exit angle of the fluid on both sides of the wake toward higher turning is observed. This effect is seen in the pitchwise distribution of absolute flow yaw angle at midspan, Fig. 18. At both rotor pitch positions of 0 and 0.3, the maxima of the exit angle are changed by up to 1 deg.

Main Flow

Reduction of Axial Velocity. The flow that is not directly affected by the rotor secondary flows is termed the main flow. It is observed that with injection, the axial velocity of the main flow at the midpitch is reduced. In Fig. 17, the distribution at the midspan shows a reduced axial velocity between rotor pitch positions of 0.3 and 1.0. This effect is also seen in the other injection configurations (see Fig. 19). The reason for this redistribution of mass flow is still under investigation.

Increased Turning. With injection, the exit angle of the rotor flow between 30% and 70% span changes toward higher turning. This effect is seen in the pitchwise mass-averaged yaw angle distribution in Fig. 15. The previously described reduction of axial velocity in this region results in the opposite effect, and is thus not the source of this increase.

Effect of the Injection Position

The injection of casing air into the rotor tip region has been investigated with three injection configurations at different axial positions:

(A) at 30% rotor axial chord
(B) at 50% rotor axial chord
(C) at 30% and 50% rotor axial chord

In the previous section, the detailed effects on the flow field have been described for the injection configuration A. In this section, the other injection configurations with 1.0% injection rate are also presented. The results are presented in terms of pitchwise mass-averaged radial distributions. In order to clarify the effect of the injection position, the differences relative to the base line case are also presented.
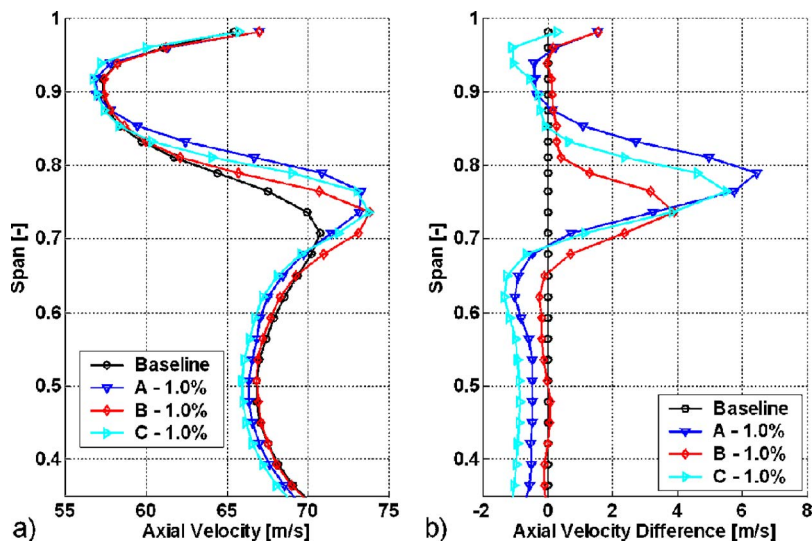
Fig. 19 Pitchwise averages of base line and three injection configurations at an injection rate of 1.0% turbine mass flow: (*a*) axial velocity (m/s) and (*b*) axial velocity difference from baseline case (m/s)

From the distribution of axial velocity presented in Fig. 19(*a*), it can be seen that the axial position of the injection has different effects. Interestingly, a more upstream injection (Case A) does not cause a deeper penetration of the cooling flow into the main flow compared to a more downstream injection (Case B). This is more clearly seen in the difference plot in Fig. 19(*b*). It is thought that the reason for this behavior is the effect the injection fluid has on the development of the rotor tip passage vortex. It has been shown above that the injection fluid accumulates mostly inside the passage vortex. Hence, depending on its radial position, an increase of axial velocity occurs.

The axial velocity distributions also show the extent of the redistribution of mass flow within the rotor passage. A more upstream injection (Case A) has the highest level of mass flow redistribution. In this case, the axial velocity is reduced in the midspan region of the wake between 30% and 70% span, whereas the axial velocity increases in the passage vortex region. A more downstream injection (Case B) shows a similar effect in the wake

region, however, a smaller effect in the vortex region. The simultaneous injection at both axial positions (Case C) shows in the region of the passage vortex values in between the other two cases, which indicates a quasilinear behavior.

The change of radial position of the rotor passage vortex, which is inferred from the distribution of axial velocity, is confirmed in the distribution of flow yaw angles (see Fig. 20). The position of the passage vortex is changed the most for the most upstream injection case. The smallest radial shift occurs at the 50% rotor axial chord injection position. From the difference plot (Fig. 20(*b*)), it can be seen that the yaw angle distributions are almost linearly related to the axial injection position. The simultaneous injection at both axial positions (Case C) results in an angle distribution that is in between the two single-row injections (Cases A and B).

The effect of the casing injection to reduce the turbulence intensity of the rotor tip vortices is evaluated for the three injection cases in Fig. 21. Also, the turbulence distributions show a quasi-
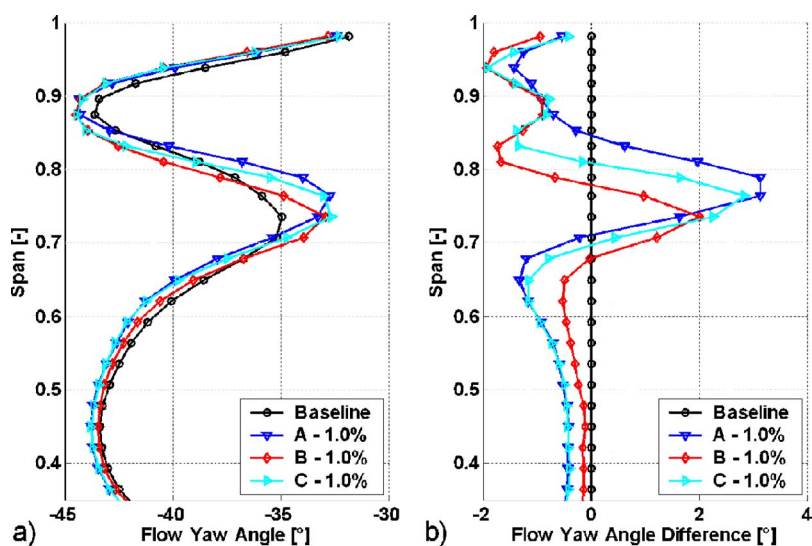

Fig. 20 Pitchwise averages of base line and three injection configurations at an injection rate of 1.0% turbine mass flow: (*a*) flow yaw angle (deg) and (*b*) flow yaw angle difference from base line case (deg)
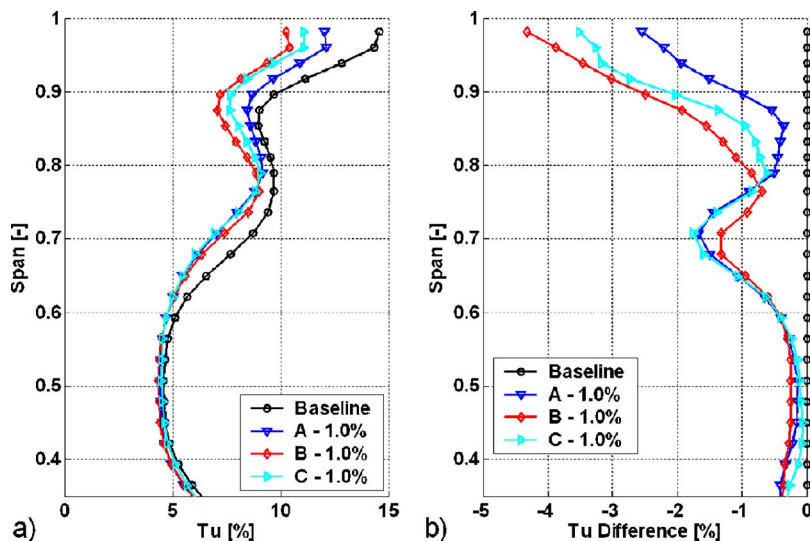
Fig. 21 Pitchwise averages of base line and three injection configurations at an injection rate of 1.0% turbine mass flow: (*a*) turbulence intensity (%) and (*b*) turbulence intensity difference from base line case (%)

linear relation to the axial injection position. The most upstream injection case yields the largest reduction of turbulence in the passage vortex. However, the same case shows a smaller reduction of turbulence in the tip region between 80% span and the casing end wall. It is thought that this behavior depends on which flow features are most affected by the casing injection. In Case A, the cross-passage flow and hence the passage vortex seem to be most changed. In Case B, the tip leakage is most affected by the casing air injection.

Discussion

The concept of injecting casing cooling air through an array of inclined holes into the tip region of a rotor increases the complexity of the flow in this region. The experimental data show that there are significant effects on the entire flow field of the rotor. Depending on where the injected air enters the rotor passage, it may attenuate or intensify the existing flow features, which are illustrated in Fig. 9.

Due to the fact that the injection is modulated by the pressure field of the rotor, a portion of the injected fluid interacts with the rotor tip leakage flow. The other portion of the flow is entrained into the cross-passage flow of the rotor, which generates the rotor tip passage vortex. Calculation of the pitchwise distribution of the injection yields a 1:1 ratio of the two mass flows. This ratio will depend on the specific turbine configuration, especially on the pitch area covered by the metal surface of the blade tip. The experiments have shown that both parts of the injected fluid can improve the aerodynamic performance of the rotor due to the mechanisms described below. Their final effect on the overall performance will be evaluated in the next section.

From the measurements of turbulence intensity, it is shown that the tip leakage vortex moves with injection closer to the rotor suction side and occupies a smaller pitch area in the rotor exit plane (see Fig. 13). In the opinion of the authors, this effect is a result of the injected air that counteracts the tip leakage flow and moves the onset of the tip leakage vortex to a more downstream position. As a result, the vortex occupies a smaller volume of the rotor passage and therefore reduces its interaction with the main flow on the blade suction side. The reduced turbulence intensity of the vortex implies a reduced level of turbulent kinetic energy, which should decrease the related loss. It is suggested that the injection stabilizes the rotating flow of the vortex, and hence causes a reduction of the turbulence intensity.

The portion of the injected air that is entrained in the cross-passage flow shows that there is potential to control the rotor tip passage vortex. The yaw angle measurements show that there is a modification of the vortex characteristic angle distribution. The increased level of overturning-underturning and the radial outward shift of this region indicate that the passage vortex is altered. Its rotational strength is increased but the diameter is reduced. As a consequence, the passage vortex moves further radial outward.

From measurements of axial flow velocity, it was concluded that the injected cooling mass flow accumulates mostly inside the tip passage vortex and the tip leakage vortex. Furthermore, probe measurements have shown an increased level of turbulent kinetic energy and temperature in the flow regions of the vortices with respect to the main flow. Downstream of the blade row, the hotter fluid of the vortex mixes with the colder fluid of the main flow. Hereby, the creation of losses is also a function of the temperature difference. The accumulation of colder air of the injection inside the vortex will reduce its temperature. Hence, the temperature gradient to the blade surface and thus the heat load on the blade as well as the mixing losses reduce.

A secondary effect of the air injection on the rotor wake and the rotor main flow is observed. It is thought that the modified shape and position of the tip leakage vortex and the tip passage vortex cause a change of the 3D pressure distribution on the rotor blade surface. Consequently, the development of the rotor wake is changed with injection, and results in a more detached position of the wake from the rotor suction side surface (see Fig. 17). In addition, the exit angle in the span region of the wake increases toward higher turning with the injection.

Performance

This section presents performance data of the injection cases investigated. On the basis of these values, the overall effect of the injection on the flow field and the performance of the turbine can be evaluated. From the turbulent velocity fluctuations of the flow, the turbulent kinetic energy (TKE) can be derived as

$$\text{TKE} = 0.5(c_{\text{sw}}^{\prime 2} + c_r^{\prime 2} + c_\theta^{\prime 2})$$

Figure 22 shows the relation between the TKE and the injection rate. The plot shows mass-averaged values in order to account for the mass flow redistribution in the flow field due to the injection. Even though the injected mass flow mainly accumulates in the vortex regions, the mass-averaged value of TKE reduces with in-
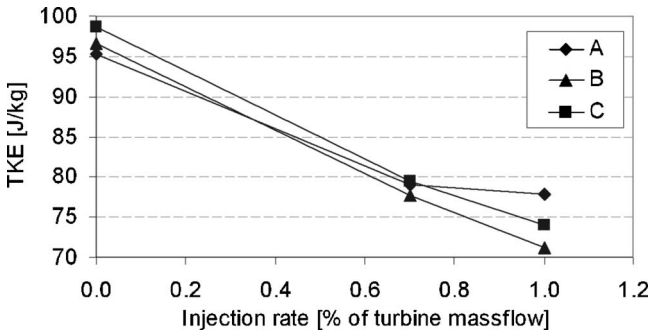
Fig. 22 TKE (J/kg) (mass averaged) versus injection rate (% of turbine mass flow)

Fig. 23 Change of isentropic efficiency (%) compared to the base line case versus injection rate (% of turbine mass flow)

jection. All three injection cases show a reduction of 20–25% at an injection rate of 1% compared to the base line.

In Ref. [28], the high turbulent flow of the rotor tip vortices could be related to a periodically appearing region of reduced total pressure at the exit of the subsequent stator. Consequently, a reduced level of turbulence of the rotor vortices is thought to have a positive effect on the generation of total pressure loss within the next stator row.

In order to evaluate the overall effect of the injection on the performance of the turbine, the efficiency of the different injection cases is analyzed. The aerodynamic efficiency can be defined as the ratio of the real and isentropic enthalpy flux difference,

$$\eta = \frac{\Delta \dot{H}_{\text{real}}}{\Delta \dot{H}_{\text{is}}} \quad \text{where } \Delta \dot{H} = \dot{m}(h_{t,\text{in}} - h_{t,\text{out}}) \text{ and } h_t = c_p T_t$$

If various mass flows of different total temperatures and pressures are involved in the expansion process, as in the case of cooling injection, a general definition can be formulated,

$$\eta = \frac{\sum_{i=1}^{I} \dot{m}_i c_p T_{t,i} - \sum_{j=1}^{J} \dot{m}_j c_p T_{t,j}}{\sum_{i=1}^{I} \dot{m}_i c_p T_{t,i} - \sum_{j=1}^{J} \dot{m}_j c_p T_{t,\text{is},j}} \quad \text{with } T_{t,\text{out,is}} = T_{t,\text{in}} \left(\frac{p_{t,\text{out}}}{p_{t,\text{in}}} \right)^{(\kappa-1)/\kappa}$$

Based on the total pressure ratio and the inlet total temperature of each mass flow, its isentropic exit temperature can be derived.

In the current cases, the turbine inlet mass flow $\dot{m}_M$ and the injection mass flow $\dot{m}_I$ introduced energy into the system. The sum of both mass flows $\dot{m}_T = \dot{m}_M + \dot{m}_I$ leaves the rotor. The total temperatures and total pressures of the passage mass flows were measured with FRAP. The 2D temperature and pressure data of each plane are mass-averaged values. The values of the injection mass flow were measured inside the plenum with three PT100 sensors and three total pressure sensors.

According to the above equations, a thermodynamic isentropic efficiency value can be defined for the current case as follows:

$$\eta = \frac{\dot{m}_M c_p \overline{T_{t,M}} + \dot{m}_I c_p \overline{T_{t,I}} - \dot{m}_T c_p \overline{T_{t,T}}}{\dot{m}_M c_p \overline{T_{t,M}} \left(1 - \frac{\overline{p_{t,T}}}{\overline{p_{t,M}}} \right)^{(\kappa-1)/\kappa} + \dot{m}_I c_p \overline{T_{t,I}} \left(1 - \frac{\overline{p_{t,T}}}{\overline{p_{t,I}}} \right)^{(\kappa-1)/\kappa}}$$

The change of efficiency of the three injection cases compared to the base line is presented in Fig. 23. The most upstream injection at 30% axial chord (Case A) achieves the maximum efficiency gain of 0.55% at the injection rate of 0.7%. At 1% injection rate, the efficiency is increased only by 0.41%. The injection at 50% axial chord (Case B) reduces the efficiency by −0.12% at 1% injection. If air is injected from both axial positions (Case C), the efficiency is in between the two single-row injections.
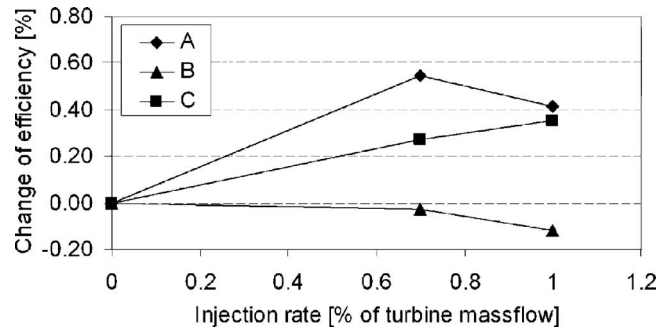
These results reflect two competing mechanisms, which influence the effect of injection on the stage efficiency. From the momentum balance on the rotor, it can be seen that the injection against the rotor turning direction reduces the torque on the rotor. The differential torque of the injection is calculated as $\Delta M_I = r_{\text{tip}} \dot{m}_I c_{I,\theta}$. If the injection mass flow is increased, the injection velocity increases proportional to that. Therefore, the differential torque of the injection on the rotor is proportional to the square of the injection mass flow, $\Delta M_I \propto \dot{m}_I^2$. At the same time, the injection causes an increase in efficiency compared to the base line case. This positive effect comes from an improved aerodynamic performance of the stage due to the reduction of secondary flow losses in the tip region of the rotor. The results of this investigation suggest that an improvement of efficiency can be achieved with an injection in the upstream part of the tip leakage and cross-passage flow development region and a moderate injection rate.

Conclusions

A novel approach of using rotor casing cooling air for the control of rotor tip secondary flows is presented. The cooling air is injected in the circumferential direction at a 30 deg angle from the casing tangent, opposing the rotor turning direction through a circumferential array of ten holes per rotor pitch. Three different cooling air injection configurations are investigated at injection rates of up to 1% of the turbine mass flow. FRAPs and fast-response wall pressure sensors were used to measure the rotor flow field.

The effects of the casing air injection on the unsteady rotor flow field are analyzed in the current paper. A flow model that describes the interaction of the injected fluid with the main flow is presented. It subdivides the interaction between injected fluid and main flow in two regions. In one region, the injected fluid counteracts with the tip leakage fluid. In the other region, the fluid is injected into the cross-passage flow and influences the development of the passage vortex.

With the casing injection, it was possible to reduce the size of the rotor tip leakage and the tip passage vortex. Both vortices move toward the tip suction side corner of the rotor passage. In accordance to the flow model, the more upstream axial injection position at 30% axial chord affected more the passage vortex, whereas the injection at 50% axial chord had more effect on the tip leakage vortex.

The turbulence intensity of the rotor tip vortices reduces with the injection. The overall TKE of the rotor exit flow field reduces linearly with the injection rate. With an injection of 1% of the turbine passage mass flow, the TKE reduces by 25% with respect to the noninjection case.

From the isentropic efficiencies of the injection cases, it can be concluded that the aerodynamic performance of the rotor improves with injection. However, the negative momentum of the injected fluid reduces the work output of the rotor. In the current study, the optimum between both effects was found at an injection

of 0.7% of the turbine mass flow at 30% axial chord, which improved the isentropic efficiency by 0.55% percentage points.

Nomenclature

c = absolute flow velocity (m/s)
v = rotor-relative velocity (m/s)
u = rotor velocity (m/s)
c_p = specific heat capacity at constant pressure (J/kg K)
h = enthalpy (J/kg)
$\dot{m}$ = mass flow (kg/s)
p = pressure (Pa)
r = radius (m)
$\dot{H}$ = enthalpy flux (W)
M = torque (N m)
T = temperature (K)
tu = turbulence intensity (%)
TKE = turbulent kinetic energy (J/kg)
C_p = pressure coefficient $C_p = (p - p_{s,3})/(p_{t,0} - p_{s,3})$
DR = density ratio (ρ_c/ρ_m)
BR = blowing ratio $(\rho_c c_c/\rho_m c_m)$
IR = momentum flux ratio (BR^2/DR)

Greek

ρ = density (kg/m^3)
η = efficiency
ψ = loading coefficient $(\psi = \Delta h/u^2)$
ϕ = flow coefficient $\phi = c_x/u$
κ = isentropic coefficient $(\kappa c_p/c_v)$
σ = standard deviation

Abbreviations

FRAP = fast-response aerodynamic probe
PS = pressure side
SS = suction side
RMS = root mean square

Subscripts

0 = turbine inlet is isentropic
3 = turbine exit
x = axial coordinate
sw = streamwise coordinate
r = radial coordinate
θ = circumferential coordinate
c = coolant jet
m = local main flow
is = isentropic
rel = rotor relative
s = static
t = total
w = wall
I = rotor injection flow
M = first stage main inlet flow
T = first stage total exit flow

Superscripts

$^{-}$ = mass average
$^{\cdot}$ = turbulent fluctuation

References

[1] Booth, T. C., Dodge, P. R., and Hepworth, H. K., 1982, "Rotor-Tip Leakage Part I-Basic Methodology," ASME J. Eng. Power, **104**, pp. 154–161.

[2] Denton, J. D., 1993, "Loss Mechanisms in Turbomachines," ASME J. Turbomach., **115**, pp. 621–656.

[3] Booth, T. C., 1985, "Importance of Tip Leakage Flows in Turbine Design," *Tip Clearance Effects in Axial Turbomachines* (VKI Lecture Series 1985-05), von Karman Institute, Rhode-St-Genèse, Belgium.

[4] Bindon, J. P., and Morphis, G., 1990, "The Development of Axial Turbine Leakage Loss for Two Profiled Tip Geometries Using Linear Cascade Data," ASME Paper No. 90-GT-152.

[5] Kaiser, I., and Bindon, J. P., 1997, "The Effect of Tip Clearance on the Development of Loss Behind a Rotor and a Subsequent Nozzle," ASME Paper No. 97-GT-53.

[6] Yoshino, S., 2002, "Heat Transfer in Rotating Turbine Experiments," Ph.D. thesis, Oxford University, Oxford.

[7] Camci, C., Dey, D., and Kavurmacioglu, L., 2003, "Tip Leakage Flows in Near Partial Squealer Rims in an Axial Flow Turbine Stage," ASME Paper No. GT2003-38979.

[8] Mischo, B., Behr, T., and Abhari, R. S., 2007, "Flow Physics and Profiling of Recessed Blade Tips: Impact on Performance and Heat Load," ASME Paper No. GT2006-91074.

[9] Chander, P., Lee, C.-P., Cherry, D., Wadia, A., and Doughty, R., "Analysis of Some Improved Blade Tip Concepts," ASME Paper No. GT2005-68333.

[10] De Cecco, S., Yaras, M. I., and Sjolander, S. A., 1995, "Measurement of Tip Leakage Flows in Turbine Cascade With Large Clearances," ASME Paper No. 95-GT-77.

[11] Yamamoto, A., Tominaga, J., Matsunuma, T., and Outa, E., 1994, "Detailed Measurements of Three-Dimensional Flows and Losses Inside an Axial Flow Turbine Rotor," ASME Paper No. 94-GT-348.

[12] Staubach, J. B., Sharma, O. P., and Stetson, G. M., 1996, "Reduction of Tip Clearance Losses Through 3-D Airfoil Designs," ASME Paper No. 96-TA-13.

[13] Offenburg, L. S., Fischer, J. D., and Hoek, T. J. V., 1987, "An Experimental Investigation of Turbine Case Treatments," Paper No. AIAA-87-1919.

[14] Harvey, N. W., 2004, "Aerothermal Implications of Shroudless and Shrouded Blades," *Turbine Blade Tip Design and Tip Clearance Treatment* (VKI Lectures Series 2004-02), von Karman Institute, Rhode-St-Genèse, Belgium.

[15] Dey, D., and Camci, C., 2000, "Development of Tip Clearance Flow downstream of a Rotor Blade With Coolant Injection From a Tip Trench," *Proceedings of the Eighth ISROMAC Conference*, Honolulu, HI, pp. 572–579.

[16] Rao, N. M., and Camci, C., 2004, "Axial Turbine Tip Desensitization by Injection From a Tip Trench, Part 1: Effect of Injection Mass Flow Rate," ASME Paper No. GT2004-53256.

[17] Rao, N. M., and Camci, C., 2004, "Axial Turbine Tip Desensitization by Injection From a Tip Trench, Part 2: Leakage Flow Sensitivity to Injection Location," ASME Paper No. GT2004-53258.

[18] Auyer, E. L., 1954, "Dynamic Sealing Arrangement for Turbomachines," U.S. Patent No. 2,685,429.

[19] Minoda, M., Inoue, S., Usui, H., and Hiroyuki, N., 1988, "Air Sealed Turbine Blades," U.S. Patent No. 4,732,531.

[20] Mischo, B., Burdet, A., Behr, T., and Abhari, R. S., 2007, "Control of Rotor Tip Leakage Through Cooling Injection From the Casing in a High-Work Turbine: Computational Investigation Using a Feature-Based Jet Model," ASME Paper No. GT2007-27669.

[21] Behr, T., Kalfas, A. I., and Abhari, R. S., 2007, "Unsteady Flow Physics and Performance of a One-and-1/2-Stage Unshrouded High Work Turbine," ASME J. Turbomach., **129**, pp. 348–359.

[22] Kupferschmied, P., Köppel, O., Gizzi, W. P., and Gyarmathy, G., 2000, "Time Resolved Flow Measurements With Fast Aerodynamic Probes in Turbomachinery," Meas. Sci. Technol., **11**, pp. 1036–1054.

[23] Pfau, A., Schlienger, J., Kalfas, A. I., and Abhari, R. S., 2002, "Virtual Four Sensor Fast Response Aerodynamic Probe (FRAP)," *Proceedings of the XVIth Bi-Annual Symposium on Measuring Techniques in Transonic and Supersonic Flows in Cascades and Turbomachines*, Cambridge, UK, Sept. 23–24.

[24] Porreca, L., Hollenstein, M., Kalfas, A. I., and Abhari, R. S., 2005, "Turbulence Measurements and Analysis in a Multistage Axial Turbine," ISABE Conference, Munich, Germany, Paper No. 2005-1032.

[25] Bernsdorf, S., Rose, M. G., and Abhari, R. S., 2006, "Modeling of Film Cooling—Part I: Experimental Study of Flow Structure," ASME J. Turbomach., **128**, pp. 141–149.

[26] Sjolander, S. A., 1997, "Overview of Tip-Clearance Effects in Axial Turbines," *Secondary and Tip Clearance Flows in Axial Turbines* (VKI Lecture Series 1997-01), Von Karman Institute for Fluid Dynamics, Rhode-St-Genèse, Belgium.

[27] Xiao, X., and Lakshminarayana, B., 2002, "Experimental Investigation of End-Wall Flow in Turbine Rotor," J. Propul. Power, **18**, pp. 1122–1123.

[28] Behr, T., Kalfas, A. I., and Abhari, R. S., 2007, "Stator Clocking Effects on the Unsteady Interaction of Secondary Flows in a 1.5-Stages Unshrouded Turbine," Seventh European Turbomachinery Conference, Athens, Greece, Paper No. B217.